A Comparison of Gaofen-2 and Sentinel-2 Imagery for Mapping Mangrove Forests Using Object-Oriented Analysis and Random Forest

Rong Zhang, Mingming Jia, Zongming Wang, Yaming Zhou, Xin Wen, Yue Tan, and Lina Cheng

***Abstract*—Mangrove forest (MF) extents and distributions are fundamental for conservation and restoration efforts. According to previous studies, both the commercial Gaofen-2 (GF-2) imagery (0.8 m spatial resolution and 4 spectral bands) and freely accessed Sentinel-2 (S2) imagery (10 m spatial resolution and 13 spectral bands) have been successfully used to map MFs. However, the efficiency and accuracy of MF mapping based on these two data is not clear, especially for large-scale applications. To address this issue, first, we developed a robust classification approach by integrating object-based image analysis (OBIA) and random forest (RF) algorithm; and then, applied this approach to GF-2 and S2 images to map the extents of MF along the entire coasts of Guangxi, China, respectively; at last, compared the efficiency and accuracy of GF-2 and S2 imagery in MF mapping. Results showed that: first, based on OBIA and RF integrated classification approach both MF maps derived from GF-2 and S2 obtained high mapping accuracies (the overall accuracy was 96% and 94%, respectively); second, areal extent of MFs in Guangxi extracted from GF-2 and S2 images was 8182 and 8040 ha, respectively; third, GF-2 imagery has extraordinary abilities in detecting fragmented MF patches located along landward and seaward edges; and finally, S2 imagery performed better in detecting seaward submerged MFs and separating MF from terrestrial vegetation. Results and conclusions of this study can provide basic considerations for selecting appropriate data source in MF or wetland vegetation mapping tasks.**

***Index Terms*—China, gaofen-2 (GF-2), mangrove forest (MF), object-based image analysis (OBIA), random forest (RF), Sentinel-2 (S2).**

Manuscript received January 10, 2021; revised March 2, 2021; accepted March 22, 2021. Date of publication April 5, 2021; date of current version April 26, 2021. The work was supported in part by the Science and Technology Basic Resources Investigation Program of China under Grant 2019FY100607, in part by The Youth Innovation Promotion Association of Chinese Academy of Sciences under Grant 2021227, in part by the Open Fund of State Laboratory of Information Engineering in Surveying, Mapping and Remote Sensing, Wuhan University under Grant 19I02, and in part by the National Earth System Science Data Center (www.geodata.cn). *(Corresponding author: Mingming Jia.)*

Rong Zhang is with the Key Laboratory of Wetland Ecology and Environment, Northeast Institute of Geography and Agroecology, Chinese Academy of Sciences, Changchun 130102, China, and also with the University of Chinese Academy of Sciences, Beijing 100049, China (e-mail: zhangrong@iga.ac.cn).

Mingming Jia is with the Key Laboratory of Wetland Ecology and Environment, Northeast Institute of Geography and Agroecology, Chinese Academy of Sciences, Changchun 130102, China (e-mail: jiamingming@iga.ac.cn).

Zongming Wang is with the Key Laboratory of Wetland Ecology and Environment, Northeast Institute of Geography and Agroecology, Chinese Academy of Sciences, Changchun 130102, China, and also with the National Earth System Science Data Center, Beijing 100101, China (e-mail: zongmingwang@iga.ac.cn).

Yaming Zhou is with the Ministry of Ecology and Environment Center for Satellite Application on Ecology and Environment, Beijing 100094, China (e-mail: zhouym@0521@163.com).

Xin Wen and Lina Cheng are with the College of Earth Sciences, Jilin University, Changchun 130061, China, and also with the Key Laboratory of Wetland Ecology and Environment, Northeast Institute of Geography and Agroecology, Chinese Academy of Sciences, Changchun 130102, China (e-mail: wenxin18@jlu.edu.cn; chengln20@mails.jlu.edu.cn).

Yue Tan is with the School of Geomatics and Prospecting Engineering, Jilin Jianzhu University, Changchun 130118, China, and also with the Key Laboratory of Wetland Ecology and Environment, Northeast Institute of Geography and Agroecology, Chinese Academy of Sciences, Changchun 130102, China (e-mail: tanyue1224@gmail.com).

Digital Object Identifier 10.1109/JSTARS.2021.3070810

I. Introduction

MANGROVE forests (MFs), as an important intermediate ecosystem, are extensively distributed in the intertidal zone along tropical and subtropical coasts [1]–[3]. These forests play a vital role in maintaining biodiversity, stabilizing shoreline, keeping water quality, preventing the storm and providing numerous societal services and goods [4], [5]. However, MFs are rapidly disappearing due to the natural and anthropogenic disturbance activities [6], [7]. Thus, an accurate and up-to-data map of MFs is essential for conservation and management efforts.

Traditionally, investigating MFs are extraordinarily difficult and time consuming due to the muddy intertidal environment [8]–[10]. Remote sensing provides opportunities for mapping MFs with the unparalleled advantages of multiscale, long-term, and cost-effective [11]–[14]. Among various satellite data, Landsat series images with long-term storage and free accessibility have been widely used for mapping MFs [12], [15], [16]. However, the Landsat's medium spatial resolution of 30 m does not allow small patches of MF to be mapped [17]. The Gaofen-2 (GF-2) satellite, which was launched on 19 August 2014 and acquired images at a spatial resolution of 0.8 m (panchromatic band) and four spectral bands (Blue, Green, Red, and Near-infrared), provides new opportunities for mapping, monitoring, and better-characterizing patchy ecosystems [18]. GF-2 imagery could provide finer spatial resolution, and more detailed information of textural structures, which could improve the ability of distinguish MFs from other adjacent vegetation [19]. Liu *et al.* [20] demonstrated that GF-2 performed better in detecting patchy vegetation than CBERS-04 (China–Brazil Earth Resources Satellite 4) and GF-1 (Gaofen-1). Liu and Chen [21] found that the textural, spectral, and multitemporal features extracted from GF-2 images could provide plenty information on intercropping regions. Nonetheless, some issues still exist in

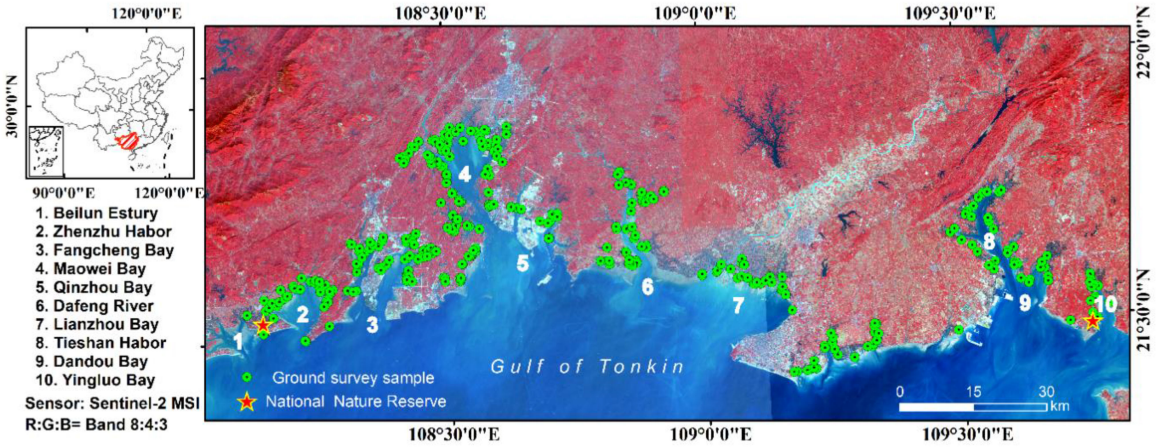

Fig. 1. Location of the study area and the distribution of ground survey sample.

mapping MFs with GF-2 images, such as the limited spectral bands, the complex preprocessing procedures, and costly price, which are common problems in very high-resolution satellite images.

Wang *et al.* [22] showed that spectral information played a more significant role in classifying mangrove species than spatial information. The recently launched Sentinel-2 (S2) satellite carrying with the multispectral instrument (MSI) sensor provides opportunities in mapping MFs at a fine spatial resolution (10 m) and 13 spectral bands. In addition, the MSI imagery contains three red edge bands, which were highly helpful in mapping submerged MFs [17]. However, several previous studies indicated that spatial resolution was more important than spectral information in identifying patchy and narrow MF [12], [23]. Kamal *et al.* [24] compared and contrasted the ability of different image datasets (Landsat TM, ALOS AVNIR-2, WorldView-2, and LiDAR) to map five levels of mangrove features, they found that higher image spatial resolution, larger object size, and less land-cover types contribute to higher mapping accuracies. Thus, given the inconstant conclusions on the relative importance of spatial and spectral resolutions in mapping MFs, and the extensive application of MF maps with high accuracy, it is necessary to investigate the performance of GF-2 and S2 images for mapping MFs.

The main objective of this study is to compare the ability of GF-2 and S2 imageries in mapping MFs on a large-scale. To achieve this goal, we develop a robust MF classification approach by integrating the object-based image analysis (OBIA) with random forest (RF) algorithm; and applying the approach to GF-2 and S2 images of Guangxi, China, respectively. The differences of the resultant maps are analyzed and compared for the advantages and limitations of GF-2 and S2 images in large-scale MF mapping.

II. Materials and Methods

A. Study Area

The coastal zones of Guangxi (21°24′20 ″- 22°01′ 20″N, 107°56′30″- 109°40′ 00″E), are close to the southwest boundary of China and 1488 km long (see Fig. 1). This study area includes two national mangrove reserves, i.e., Shankou National Mangrove Nature Reserve and Beilun Estuary National Nature Reserve. The dominant mangrove species in Guangxi are *Avicennia marina*, *Aegiceras corniculatum*, *Kandelia candel*, *Bruguiear gymnorrhiza,* and *Rhizophora stylosa*. Almost 98.8% of MFs in Guangxi are shorter than 4m [25]. The MFs in Guangxi account for approximately 37% of national total MFs and present large integral patches, narrow patches, and fragmented patches [15]. In this study, we defined small mangrove patch as the patch of MF with an area of less than 500 m^2.

TABLE I
Characteristics of Satellite Data and Image Acquisition Dates

Imagery	Acquisition dates	Band number and name	Wavelength (nm)	Resolution (m)
Gaofen-2	May 16 to Sep. 21, 2016	1 Pan	450-900	0.8
	May 16 to Dec. 21, 2017	2 Blue	450-520	4
		3 Green	520-590	4
		4 Red	630-690	4
		5 NIR	770-890	4
Sentinel-2	17 December 2017	2 Blue	398–594	10
	19 December 2017	3 Green	515–605	10
		4 Red	626–702	10
		5 Red edge	695–710	20
		6 NIR1	730–740	20
		7 NIR2	768–796	20
		8 NIR3	690–980	10
		8a NIR4	848–881	20
		11 SWIR1	1470–1756	20
		12 SWIR2	1960–2444	20

B. Remote Sensing Data

A complete coverage of the Guangxi coasts was achieved by 15 tiles of GF-2 paths/rows or 5 tiles of S2 paths/rows. The spatial locations and general information of GF-2 images and S2 spectral bands are shown in Table I and Fig. 2. GF-2 is an optical remote sensing satellite developed by China. This satellite is equipped with panchromatic and multispectral sensor, with a 0.8 m resolution panchromatic band and four 4 m resolution

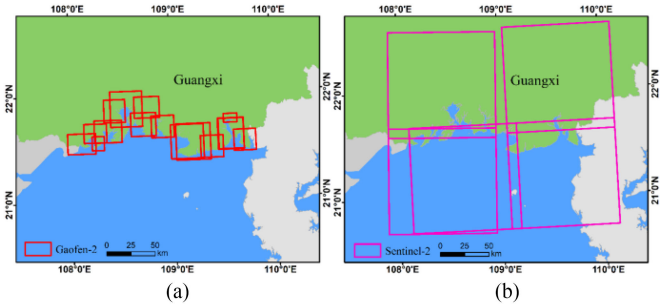

Fig. 2. Coverage regions of images for the entire coast of Guangxi. (A) Spatial distributions of GF-2 images; (B) Spatial distributions of S2 images.

multispectral bands covering the spectral ranges between visible (VIS) and the near-infrared (NIR) (see Table I). The GF-2 images were provided by the National Satellite Oceanic Application Center, China.[1] The data need a series of preprocessing before applied for MF classification. First, orthorectification were conducted based on the ENVI rational polynomial coefficients (RPC) with 30 equally distributed ground control points extracted from a 1:100000 topographic maps. Then, atmospheric corrections were carried out for both GF-2 images by applying the dark object subtraction algorithm. Finally, the spatial resolution of multispectral images was enhanced to 0.8 m after the nearest neighbor diffusion pan-sharpening algorithm was applied to image fusion. Orthorectification, atmospheric corrections, and image fusion were performed using ENVI (Exelis Visual Information Solutions, Boulder, CO, version 5.3).

Low cloud-cover S2 images, acquired between December 17 and 19, 2017 (see Table I and Fig. 2) were downloaded from "Copernicus Open Access Hub" webpage[2] as Level-1C product, i.e., top-of-atmosphere reflectance in cartographic geometry. Atmospheric correction was conducted using Sen2cor module version 2.5.5 within the S2 Toolbox of SNAP (Sentinel Application Platforms, version 6.4) [26].

C. Reference Data

Field surveys were carried out during the period of November 1–15, 2017. Intertidal MFs were surveyed along walkways with the guidance of local guidepost. The location of each field point was established by global positioning system with an accuracy of less than 1 m, and recorded for the species names. Because most of the mudflat areas of MFs were inaccessible, we also collected ground survey samples by Google Earth and unmanned aerial vehicles. As a result, 437 mangrove forest ground survey samples and 650 non-MF ground survey samples were selected. Then, the points were randomly divided into two groups for the purpose of image validation (237 validation samples) and classification (200 training samples).

D. Methodology

1) Basic Idea of OBIA and RF Classification: Extensive research works showed that OBIA was superior to pixel-based methods in MF mapping, particularly for high-resolution images applications [27], [28]. Classification algorithms, such as maximum likelihood, support vector machines, neural networks, and RF, are used to classify image objects. Among these algorithms, the RF algorithm has been widely employed due to its accurate and robust performances [29], [30]. To date, the RF algorithm along with OBIA is still rarely used in mapping MFs, large-scale applications need to be explored [31], [32].

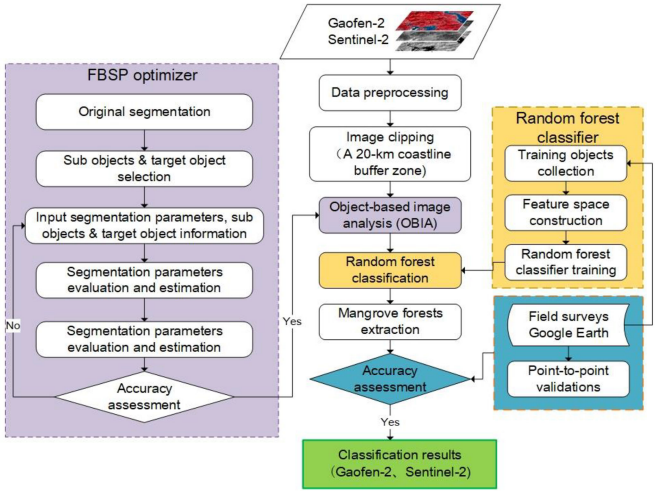

Fig. 3. Workflow for mapping mangrove forests includes OBIA, RF, and accuracy assessment. The coastline was provided by Hou *et al.* [33].

In this study, the general workflow of MF classification includes three steps (see Fig. 3).

1) Segmenting images into objects using the fuzzy-based segmentation parameter (FBSP) optimizer.
2) Classifying objects into MF and non-MF using RF classifier.
3) Evaluating the classification accuracy. In this manuscript, we used a 20-km coastline buffer zone to clip the images, the coastline was provided by Hou *et al*. [33].

2) Image Segmentation Based on FBSP Optimizer: Image segmentation directly influences the efficiency and accuracy of classification results [34]. In this study, GF-2 and S2 images were segmented into homogeneous objects using multiresolution segmentation, which is one of the most useful segmentation algorithms, implemented in the eCognition Developer software (version 9.0). Multiresolution segmentation is a bottom-up region merging algorithm, starts with the pixel level and iteratively merges pixels into objects based on the conditions of homogeneity (similarity of spatial and spectral information) set by users [35]. The conditions include three parameters: scale, shape, and compactness. In general, multiresolution segmentation parameters are often dependent on subjective trial-and-error methods [36]. In order to obtain segment parameters, we used an automated tool for segmentation, namely FBSP optimizer [37]. The algorithm of the FBSP optimizer is based on the idea of discrepancy evaluation, which evaluates effectiveness for the process of merging subobjects with fuzzy logic analysis [38]. Examples of original multiresolution segmentation and optimal

[1]http://dds.nsoas.org.cn/mainIndex.do
[2]https://scihub.copernicus.eu/dhus/#/home

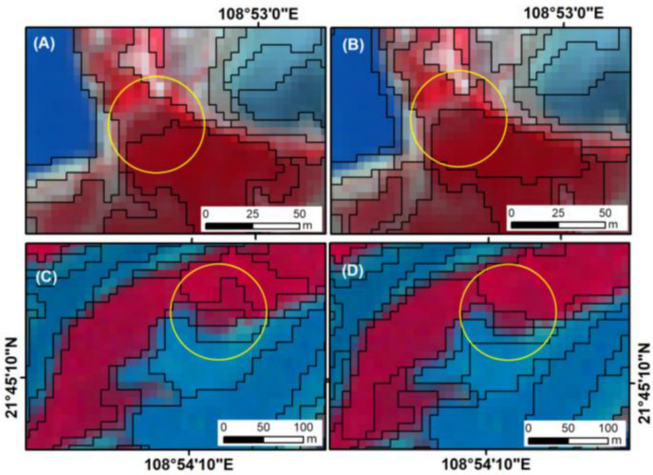

Fig. 4. Comparison of original multiresolution segmentation and optimal multiresolution segmentation. (A) Original segmentation of GF-2, the parameter of scale, shape and compactness is 25, 0.10, and 0.50, respectively. (B) Optimal segmentation of GF-2, the parameter of scale, shape, and compactness is 21, 0.18, and 0.74, respectively. (C) Original segmentation of S2, the parameter of scale, shape, and compactness is 25, 0.10, and 0.50, respectively. (D) Optimal segmentation of S2, the parameter of scale, shape, and compactness is 20, 0.17, and 0.75, respectively.

multiresolution segmentation are presented in Fig. 4. The optimal multiresolution segmentation retained useful information and reduced redundant objects. Therefore, it could efficiently improve classification accuracy and reduce the workloads.

3) RF Classification: RF is an ensemble learning algorithm, which has been confirmed accurate and robust in image classification [29], [30], [32]. In this study, RF was run in eCognition Developer software (version 9.0).

In order to generate a RF prediction model, two important parameters need to be defined: first, the number of decision trees (ntree), which will be established by randomly selecting samples from the training samples; and second, the number of predictive variables (mtry), which defines the best partition in each node of decision trees. Research works such as that conducted by Lawrence *et al.* (2006) have shown that the number of error models tends to be stable beyond the creation of 1000 decision trees from randomly selecting samples [41]. Data from several studies suggest that the value of the parameter mtry was set as the square root of the number of the input features [41], [42].

A plenty of features can be adopted as input variables in RF classifier, including spectral, spatial, and temporal features. Fortunately, the OBIA could provide a number of spatial features over pixel-based methods. In this article, 33 spectral and spatial features were selected as input variables in the RF classifier (see Table II).

4) Validation of the MF Maps: To validate mapping accuracies, we derived two confusion matrices based on ground survey samples, and calculated overall accuracies and F1 scores of different MF maps. Overall accuracy represents to the correct proportion of mapped compared with ground points. F1 score is a harmonic mean of user's accuracy (UA) and producer's accuracy (PA), which represents the classification performance of a single class [43].

TABLE II
FEATURES USED IN THE HIERARCHICAL RF CLASSIFICATION

Feature type I	Feature type II	Object feature
Spectral feature	Spectral band	Mean value of band 2, 3, 4, 5, 6, 7, 8, 8a, 11 and 12; Standard deviation of band 2, 3, 4, 5, 6, 7, 8, 8a, 11 and 12
Spatial feature	Texture	GLCM Homogeneity, GLCM Contrast, GLCM Entropy, GLCM Mean, GLCM Standard deviation, GLCM Correlation, GLCM Dissimilarity, GLDV Entropy, GLDV Mean, GLDV Contrast
	Shape	Border index, Compactness, Shape index

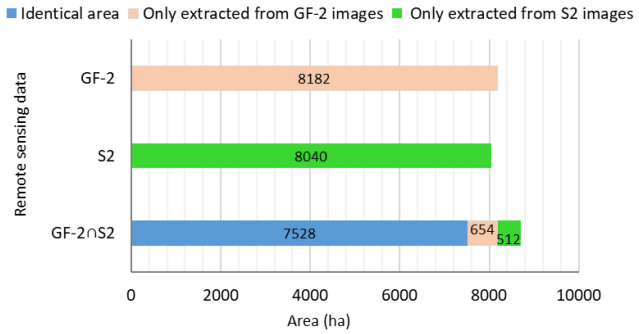

Fig. 5. Area of Guangxi mangrove forests derived from GF-2 and S2 images. The identical area represents the spatially consistent mangrove forest area among the two imageries; MF represents MFs.

III. RESULTS

A. Accuracy Assessment

Table III presents the confusion matrices for MF maps derived from GF-2 and S2. The overall accuracy of the GF-2 and S2 derived MF maps was 96% and 94%, respectively, the F1 score was 0.93 and 0.90, respectively. The MF map derived from GF-2 images had a UA and PA of 95% and 92%, respectively. MF map derived by S2 images had a UA and PA of 93% and 89%, respectively. Accuracy assessments indicated that the MF maps generated from GF-2 and S2 images both had high mapping accuracies with the map from GF-2 being more accurate.

B. Areal Extents and Spatial Distributions of MFs Extracted From GF-2 and S2

Areal extents of Guangxi's MFs derived from GF-2 and S2 are illustrated in Fig. 5. Using GF-2 and S2 imagery we mapped 8182 and 8040 ha of mangrove forests along the entire coasts of Guangxi, respectively. MFs that were identified by both GF-2 and S2 imagery were 7528 ha. In addition, 654 and 512 ha of MFs could only be identified by GF-2 and S2 imagery, respectively. We compared our mapping result with results from the State Forestry Administration (SFA) [44] and Hu *et al.* [45]. Our result was close to the SFA's (8781 ha), which was obtained by interpreting high-resolution satellite images and field surveys, and much higher than the area of Hu *et al.* (7089 ha).

The spatial distributions of MF in Guangxi are shown in Fig. 6(A). Generally, the MF mapped with GF-2 and S2 images were highly consistent. Large patches of MF were concentrated

TABLE III
CONFUSION MATRICES OF MF MAPS DERIVED BY GF-2 AND S2

		MF	Non-MF	classification Total	User's accuracy	Producer's accuracy	F1 score	Overall accuracy
Gaofen-2	MF	226	11	237	0.95	0.92	0.93	0.96
	Non-MF	19	517	536	0.96	0.98		
Sentinel-2	MF	219	18	237	0.92	0.89	0.90	0.94
	Non-MF	27	509	536	0.95	0.97		

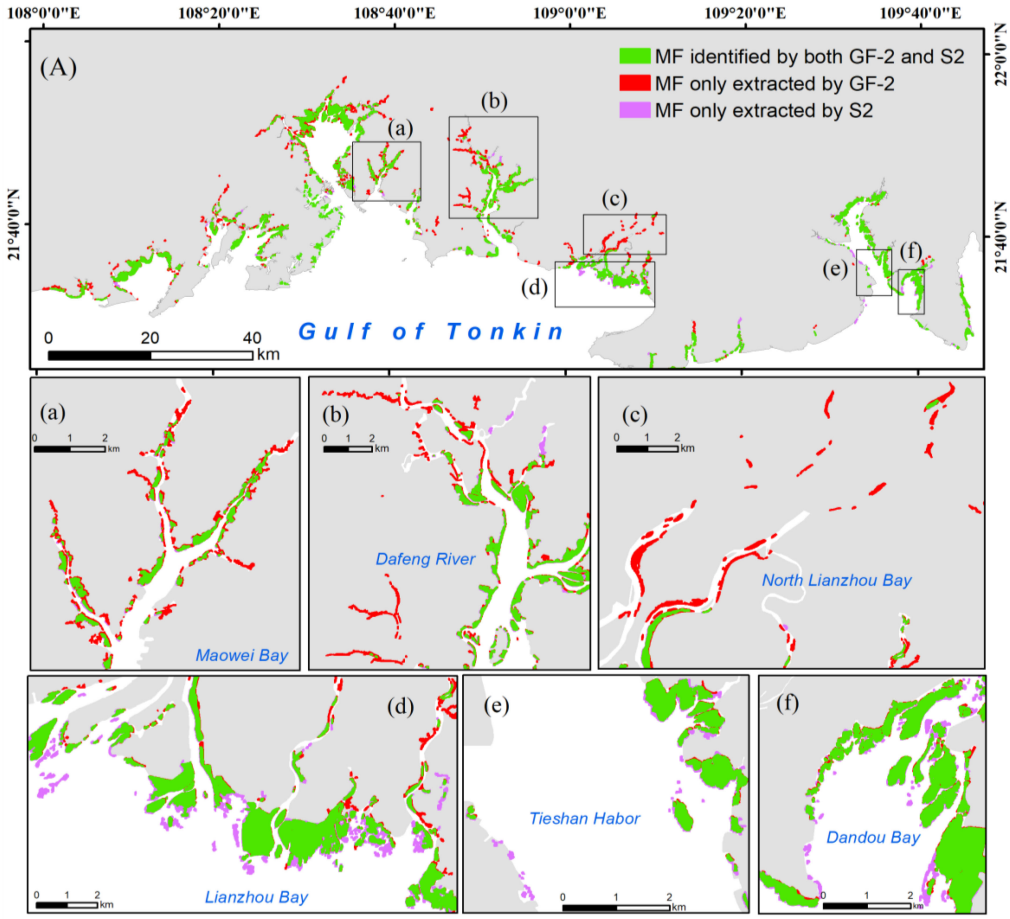

Fig. 6. (a) Spatial distribution of MF derived from GF-2 and S2 images in Guangxi, and zoom views of Maowei Bay. (b) Dafeng River. (c) North Lianzhou Bay. (d) Lianzhou Bay. (e) Tieshan Habor). (f) Dandou Bay.

in Zhenzhu Habor, Fangcheng Bay, Maowei Sea, Dafeng River, Lianzhou Bay, Tieshan Habor, and Dandou Bay. Maowei Sea had the largest amount of MF (according to the GF-2 derived map, there were 2079 ha of MF, accounting for 25% of the total), followed by Tieshan Habor (according to the GF-2 derived map, there were 1037 ha, accounting for 13% of the total) and Lianzhou Bay (according to the GF-2 derived map, there were 1002 ha, accounting for 12% of the total). Fragmented patches of MF were found in Beilun Estuary and Yingluo Bay along the eastern coasts of Guangxi.

As shown in Fig. 6(a)–(c), GF-2 images performed better than S2 images when detecting small patches along the landward and seaward edges of MF. As shown in Fig. 6(d)–(f), S2 images performed better in delineating seaward submerged MF and landward MF adjacent to terrestrial vegetation (TV).

IV. DISCUSSION

A. Reliability of Integrating OBIA and RF Classification Approach

The maps derived from GF-2 and S2 both achieved high accuracies (96% and 94%, respectively). The successful implementation of this study could be attributed to two factors, i.e., the FBSP optimizer applied in image segmentation, and the robust approach which integrated OBIA and RF.

First, FBSP optimizer was used to select optimal segmentation parameters in this study. Compared to previous approaches, the FBSP optimizer enable process image with unlimited band images and implements automated optimizing for all the segmentation parameters (i.e., scale, compactness, and shape). The FBSP optimizer, which is a supervised process, could

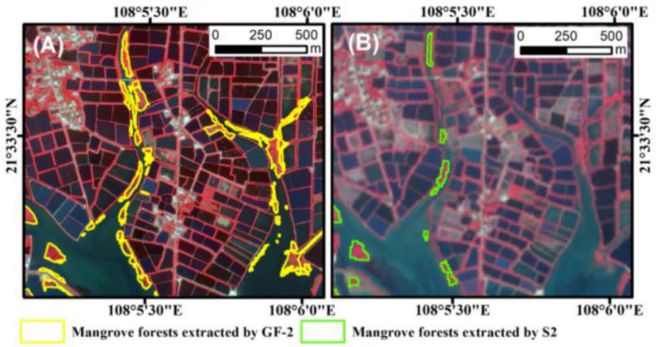

Fig. 7. Compared the results of mangrove forests extracted from (A) GF-2 (R: G: B = 4:3:2) and (B) S2 (R: G: B = 8:4:3) images in Guangxi.

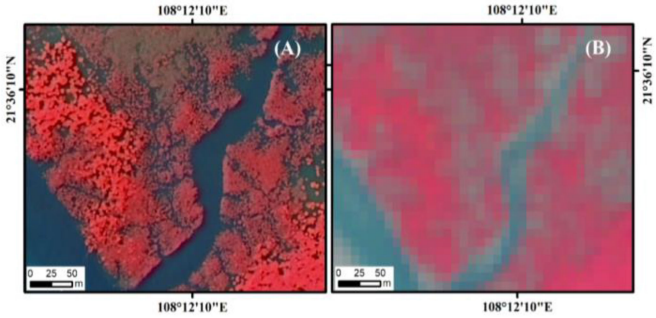

Fig. 8. Visual comparison of (A) Gaofen-2 (R: G: B=4:3:2) and (B) Sentinel-2 (R: G: B=8:4:3) image with texture coarseness.

automatically identify suitable segmentation parameters based on fuzzy logic analysis [37], [38]. This approach is accommodated in eCognition by acquiring target object and subobject features and iterative operation with fuzzy logic analyses in a bottom-up approach. The automation of the parameter selection is a significant advantage that guarantees the classification process time-efficient and accurate, and avoids subjective errors caused by trial-and-error optimization.

Second, the integration of OBIA and RF captures abundant information on the spectral and texture characteristics of MF. OBIA effectively avoids the effect of "salt-and-pepper" in a heterogeneous landscape and ensures the classification accuracy in complicated environments. The RF classifier has been shown to be the robust and stable and outperforms with other machine learning algorithms [46]–[48].

B. Advantages and Limitations of GF-2 Imagery in Mapping MFs

GF-2 images have an extraordinary ability in detecting fragmented patches of MF and delineating the boundary of MF compared with S2 images, due to the much higher spatial resolution. As shown in Fig. 7, MF located along the river can only be accurately identified by GF-2 images. Moreover, the boundary of MF was more integrally delineated by GF-2 images than S2 images. A previous study also indicated that a higher spatial resolution can improve the mapping of small patchy MF [24].

Many research works have substantiated the benefit of texture information in identifying MF [49], [50]. Concerning texture information, GF-2 images could provide abundant details of MF objects (e.g., patch structure and component). Table IV and Fig. 8 were provided to illustrate the differences of texture features derived from the GF-2 and S2 images. A total of six of text features were used: *homogeneity*, *contrast*, *dissimilarity*, *standard deviation*, *mean* and *entropy*. The *contrast* of texture features is one of the most representative features in texture image analysis. The *contrast* feature is a measure of the contrast or the amount of local variations present in an image [51]. As shown in Table IV, the values of gray-level cooccurrence matrix (GLCM) *contrast* and gray level difference vector (GLDV) *contrast* in GF-2 image are much higher than S2 image, indicating that GF-2 images provide abundant texture information. As shown in Fig. 8, for MF objects the GF-2 images exhibited more textural roughness than the S2 images.

Fig. 9 shows the spectral curves of MF, tidal flat (TF), water, TV, and submerged MF (SMF) in GF-2 and S2 images. As shown in Fig. 9(A), the spectral reflectance values of MF are slightly different from that of TV and TF in the GF-2 near-infrared band (770–890 nm). However, the reflectance in the near-infrared band (770–890 nm) is largely reduced when MF are submerged [17]. In the GF-2 images, the spectral reflectance of SMF is confused with TV and water in the visual spectral band, and is indistinguishable from TF in the near infrared band [see Fig. 9(A)]. In consequence, it is difficult to identify SMF from GF-2 images.

To sum up, GF-2 images have outstanding advantages of identifying small patches of MF and could adequately and detailed depict the boundaries of MF patches. However, due to the limited spectral bands, GF-2 images are not suitable for detecting SMF.

C. Advantages and Limitations of S2 Imagery in Mapping MF

As shown in Fig. 6(d)–(f), S2 images had an excellent performance for identifying submerged mangrove patches and landward MF adjacent to TV. As shown in Fig. 9(B), the shortwave infrared reflectance of MF is lower than that of TV, and MF show higher reflectance in the spectral region of 733–890 nm than TV. Jia *et al.* [17] analyzed the typical spectral curves of water, emerged MF, and SMF, and found that S2 could be used to detect SMF.

Previous studies indicated that it is difficult to identify MF adjacent to TV [52]. Fortunately, S2 imagery could be used to separate MF from TV [17], [31]. However, S2 images have limitations in identifying small patches of MF compared with GF-2 images. Because small patches can form mixed pixels in S2 images, which was also demonstrated by Wang *et al.* [53]. Their studies found that due to the mixed reflectance spectral of MF, TF, and waters in one pixel in S2 images, the small MF patches were dissolved within the major surrounding land cover. As a result, a large number of small patches could not been recognized in S2 images [see Fig. 6(a)–(c)].

In conclusion, S2 images have obvious advantages in identifying MF, which are submerged or adjacent to TV, but have limited abilities in detecting small MF patches.

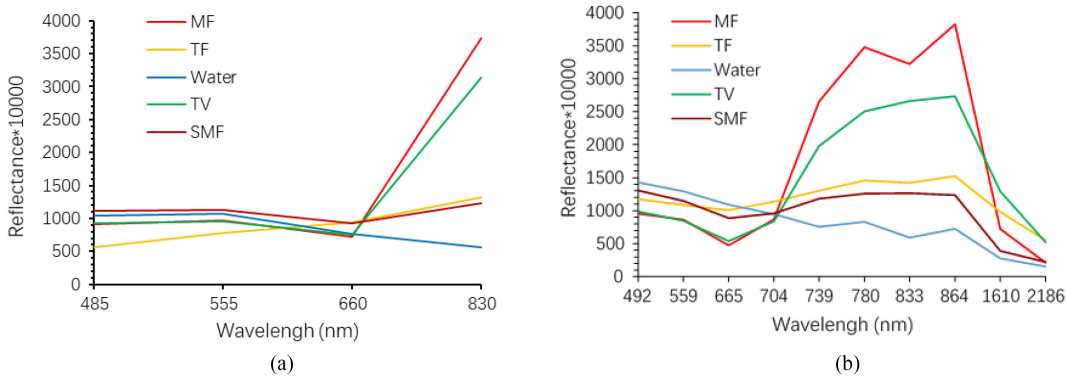

Fig. 9. Spectral curves of MF, TF, water, TV, and SMF. (a) GF-2 image. (b) S2 image.

TABLE IV
TEXTURE FEATURE OF MFS COMPARISON BETWEEN GF-2 AND S2

Texture feature	GF-2			S2		
	Min	Max	Mean	Min	Max	Mean
GLCM Homogeneity	0	0.30	0.07	0	0.23	0.05
GLCM Contrast	169.44	50019.23	6514.09	138.66	50019.23	1797.07
GLCM Dissimilarity	10.73	196.15	45.87	8.38	196.15	24.48
GLCM StdDev	11.25	124.06	46.01	11.79	124.06	24.83
GLCM Mean	85.00	137.23	123.41	98.08	137.23	123.75
GLCM Entropy	0.68	8.47	6.08	1.07	:6.83	5.48
GLDV Mean	10.73	196.15	45.87	8.38	196.15	24.48
GLDV Contrast	169.44	50019.23	6514.09	138.66	50019.23	1797.07

V. CONCLUSION

In this study, MFs have been mapped by applying an OBIA and RF integrated classification approach to GF-2 and S2 images, respectively. The overall accuracy for the GF-2 and S2 images derived MF maps was 96% and 94%, respectively. The results indicated that both GF-2 and S2 images can be used to accurately map MF. Moreover, we found that: first, small patchy MFs can be delineated with more details by GF-2 images, whereas GF-2 images have limitations in detecting SMFs; and second, S2 images have advantages in identifying MFs, which are submerged or adjacent to TV, whereas S2 images are limited in detecting small patchy MFs. Based on the results from this study, low tide GF-2 images are recommended to use for mapping fragmented MF, if the budget is adequate. In contrast, S2 images are recommended based on their relatively high mapping accuracy and free accessibility if the budget is limited or MFs are not very patchy. The proposed approach and present results are of great significance for mapping and monitoring MFs and for the selection of remote sensing data in such mapping tasks.

ACKNOWLEDGMENT

The authors would like to thank the comments of reviewers. They would like to thank Dr. X. Guo from Xiamen University for his field surveys.

REFERENCES

[1] X. Zhang *et al.*, "Mapping mangrove forests using multi-tidal remotely-sensed data and a decision-tree-based procedure," *Int. J. Appl. Earth Obs. Geoinf.*, vol. 62, pp. 201–214, 2017.
[2] D. Yin and L. Wang, "Individual mangrove tree measurement using UAV-based LiDAR data: Possibilities and challenges," *Remote Sens. Environ.*, vol. 223, pp. 34–49, 2019.
[3] H. Li, M. Jia, R. Zhang, Y. Ren, and X. Wen, "Incorporating the plant phenological trajectory into mangrove species mapping with dense time series Sentinel-2 imagery and the google earth engine platform," *Remote Sens.,* vol. 11, no. 21, 2019, Art. no. 2479.
[4] L. Wang, M. Jia, D. Yin, and J. Tian, "A review of remote sensing for mangrove forests: 1956–2018," *Remote Sens. Environ.*, vol. 231, 2019, Art. no. 111223.
[5] C. Giri *et al.*, "Distribution and dynamics of mangrove forests of south asia," *J. Environ. Manage.*, vol. 148, pp. 101–111, 2015.
[6] C. Giri *et al.*, "Status and distribution of mangrove forests of the world using earth observation satellite data," *Global Ecol. Biogeography,* vol. 20, no. 1, pp. 154–159, 2011.
[7] N. Thomas, R. Lucas, P. Bunting, A. Hardy, A. Rosenqvist, and M. Simard, "Distribution and drivers of global mangrove forest change, 1996–2010," *PLoS One*, vol. 12, no. 6, 2017, Art. no. e0179302.
[8] T. D. Pham, N. Yokoya, D. T. Bui, K. Yoshino, and D. A. Friess, "Remote sensing approaches for monitoring mangrove species, structure, and biomass: Opportunities and challenges," *Remote Sens.,* vol. 11, no. 3, 2019, Art. no. 230.
[9] N. Thomas, P. Bunting, R. Lucas, A. Hardy, A. Rosenqvist, and T. Fatoyinbo, "Mapping mangrove extent and change: A globally applicable approach," *Remote Sens.,* vol. 10, no. 9, 2018, Art. no. 1466.
[10] C. Giri, "Observation and monitoring of mangrove forests using remote sensing: Opportunities and challenges," Multidisciplinary Digital Publishing Institute, 2016.

[11] J. Tian *et al.*, "Comparison of UAV and worldview-2 imagery for mapping leaf area index of mangrove forest," *Int. J. Appl. Earth Obs. Geoinf.,* vol. 61, pp. 22–31, 2017.

[12] M. Kamal, S. Phinn, and K. Johansen, "Assessment of multi-resolution image data for mangrove leaf area index mapping," *Remote Sens. Environ.*, vol. 176, pp. 242–254, 2016.

[13] C. Kuenzer, A. Bluemel, S. Gebhardt, T. V. Quoc, and S. Dech, "Remote sensing of mangrove ecosystems: A review," *Remote Sens.,* vol. 3, no. 5, pp. 878–928, 2011.

[14] T. D. Pham, N. Yokoya, D. T. Bui, K. Yoshino, and D. Friess, "Remote sensing approaches for monitoring mangrove species, structure, and biomass: Opportunities and challenges," *Remote Sens.,* vol. 11, no. 3, 2019, Art. no. 230.

[15] M. Jia, Z. Wang, Y. Zhang, D. Mao, and C. Wang, "Monitoring loss and recovery of mangrove forests during 42 years: The achievements of mangrove conservation in China," *Int. J. Appl. Earth Obs. Geoinf.,* vol. 73, pp. 535–545, 2018.

[16] V. Otero, R. Van De Kerchove, B. Satyanarayana, H. Mohd-Lokman, R. Lucas, and F. Dahdouh-Guebas, "An analysis of the early regeneration of mangrove forests using landsat time series in the Matang mangrove forest reserve, peninsular Malaysia," *Remote Sens.,* vol. 11, no. 7, 2019, Art. no. 774.

[17] M. Jia, Z. Wang, C. Wang, D. Mao, and Y. Zhang, "A new vegetation index to detect periodically submerged mangrove forest using single-tide Sentinel-2 imagery," *Remote Sens.,* vol. 11, no. 17, 2019, Art. no. 2043.

[18] B. Tian *et al.*, "Mapping thermokarst lakes on the Qinghai–tibet plateau using nonlocal active contours in Chinese Gaofen-2 multispectral imagery," *IEEE J. Sel. Topic Appl. Earth Observ.*, vol. 10, no. 5, pp. 1687–1700, May 2017.

[19] Q. Xia, C.-Z. Qin, H. Li, C. Huang, and F.-Z. Su, "Mapping mangrove forests based on multi-tidal high-resolution satellite imagery," *Remote Sens.,* vol. 10, no. 9, 2018, Art. no. 1343.

[20] Q. Liu, C. Huang, G. Liu, and B. Yu, "Comparison of CBERS-04, GF-1, and GF-2 satellite panchromatic images for mapping quasi-circular vegetation patches in the Yellow river delta, China," *Sensors*, vol. 18, no. 8, 2018, Art. no. 2733.

[21] P. Liu, and X. Chen, "Intercropping classification from GF-1 and GF-2 satellite imagery using a rotation forest based on an SVM," *ISPRS Int. Geo-Inf.*, vol. 8, no. 2, 2019, Art. no. 86.

[22] L. Wang, W. P. Sousa, P. Gong, and G. Biging, "Comparison of IKONOS and quickbird images for mapping mangrove species on the Caribbean coast of Panama," *Remote Sens. Environ.*, vol. 91, no. 3-4, pp. 432–440, 2004.

[23] L. Valderrama-Landeros, F. Flores-de-Santiago, J. Kovacs, and F. Flores-Verdugo, "An assessment of commonly employed satellite-based remote sensors for mapping mangrove species in mexico using an NDVI-based classification scheme," *Environ. Monitoring Assessment*, vol. 190, no. 1, pp. 1–13, 2018.

[24] M. Kamal, S. Phinn, and K. Johansen, "Object-based approach for multi-scale mangrove composition mapping using multi-resolution image datasets," *Remote Sens.,* vol. 7, no. 4, pp. 4753–4783, 2015.

[25] M. Jia, Z. Wang, Y. Zhang, C. Ren, and K. Song, "Landsat-based estimation of mangrove forest loss and restoration in Guangxi province, China, influenced by human and natural factors," *IEEE J. Sel. Top. Appl. Earth Observ.*, vol. 8, no. 1, pp. 311–323, Jan. 2015.

[26] M. Jia, Z. Wang, D. Mao, C. Ren, C. Wang, and Y. Wang, "Rapid, robust, and automated mapping of tidal flats in China using time series Sentinel-2 images and Google Earth Engine," *Remote Sens. Environ.*, vol. 255, 2021, Art. no. 112285.

[27] M. Kamal and S. Phinn, "Hyperspectral data for mangrove species mapping: A comparison of pixel-based and object-based approach," *Remote Sens.,* vol. 3, no. 10, pp. 2222–2242, 2011.

[28] D. C. Duro, S. E. Franklin, and M. G. Dubé, "A comparison of pixel-based and object-based image analysis with selected machine learning algorithms for the classification of agricultural landscapes using SPOT-5 HRG imagery," *Remote Sens. Environ.*, vol. 118, pp. 259–272, Mar 15 2012.

[29] M. Belgiu and L. Drăguţ, "Random forest in remote sensing: A review of applications and future directions," *ISPRS-J. Photogramm. Remote Sens.*, vol. 114, pp. 24–31, Apr 2016.

[30] P. O. Gislason, J. A. Benediktsson, and J. Sveinsson, "Random forests for land cover classification," *Pattern Recognit. Lett.*, vol. 27, no. 4, pp. 294–300, 2006.

[31] C. Lu *et al.*, "Dynamic analysis of mangrove forests based on an optimal segmentation scale model and multi-seasonal images in Quanzhou bay, China," *Remote Sens.,* vol. 10, no. 12, 2018, Art. no. 2020.

[32] R. Gibson, T. Danaher, W. Hehir, and L. Collins, "A remote sensing approach to mapping fire severity in south-eastern Australia using Sentinel 2 and random forest," *Remote Sens. Environ.*, vol. 240, 2020, Art. no. 111702.

[33] X. Hou, T. Wu, W. Hou, Q. Chen, Y. Wang, and L. Yu, "Characteristics of coastline changes in Mainland China since the early 1940s," *Sci. China Earth Sci.*, vol. 59, no. 9, pp. 1791–1802, 2016.

[34] R. P. Powers, G. J. Hay, and G. Chen, "How wetland type and area differ through scale: A GEOBIA case study in Alberta's Boreal plains," *Remote Sens. Environ.*, vol. 117, pp. 135–145, 2012.

[35] M. Liu *et al.*, "Rapid invasion of spartina alterniflora in the coastal zone of Mainland China: New observations from Landsat OLI images," *Remote Sens.,* vol. 10, no. 12, 2018, Art. no. 1933.

[36] D. Ming, J. Li, J. Wang, and M. Zhang, "Scale parameter selection by spatial statistics for GEOBIA: Using mean-shift based multi-scale segmentation as an example," *ISPRS-J. Photogramm. Remote Sens.,* vol. 106, pp. 28–41, 2015.

[37] Y. Zhang, T. Maxwell, H. Tong, and V. Dey, "Development of a supervised software tool for automated determination of optimal segmentation parameters for ecognition," in *ISPRS TC VII Symposium - 100 Years ISPRS*, Vienna, Austria, IAPRS, 2010, pp. 690–696.

[38] H. Tong, T. Maxwell, Y. Zhang, and V. Dey,"A supervised and fuzzy-based approach to determine optimal multi-resolution image segmentation parameters," *Photogramm. Eng. Remote Sens.*, vol. 78, no. 10, pp. 1029–1044, 2012.

[39] C. Pelletier, S. Valero, J. Inglada, N. Champion, and G. Dedieu, "Assessing the robustness of random forests to map land cover with high resolution satellite image time series over large areas," *Remote Sens. Environ.*, vol. 187, pp. 156–168, 2016.

[40] R. L. Lawrence, S. D. Wood, and R. L. Sheley, "Mapping invasive plants using hyperspectral imagery and Breiman cutler classifications (Random forest)," *Remote Sens. Environ.*, vol. 100, no. 3, pp. 356–362, 2006.

[41] M. Belgiu and O. Csillik, "Sentinel-2 cropland mapping using pixel-based and object-based time-weighted dynamic time warping analysis," *Remote Sens. Environ.*, vol. 204, pp. 509–523, 2018.

[42] F. Vuolo, M. Neuwirth, M. Immitzer, C. Atzberger, and W. Ng, "How much does multi-temporal Sentinel-2 data improve crop type classification?," *Int. J. Appl. Earth Obs. Geoinf.,* vol. 72, pp. 122–130, 2018.

[43] J. Tian *et al.*, "Development of spectral-phenological features for deep learning to understand spartina alterniflora invasion," *Remote Sens. Environ.*, vol. 242, 2020, Article no. 111745.

[44] S. F. Administration, "Types and areal extent of wetlands," in *China Wetlands Resources Guangxi Volume*, Beijing, China: China Forestry Publishing House, (in Chinese), 2015, pp. 6–15.

[45] L. Hu, W. Li, and B. Xu, "Monitoring mangrove forest change in china from 1990 to 2015 using Landsat-derived spectral-temporal variability metrics," *Int. J. Appl. Earth Obs. Geoinf.,* vol. 73, pp. 88–98, 2018.

[46] A. Ghosh and P. K. Joshi, "A comparison of selected classification algorithms for mapping bamboo patches in lower Gangetic plains using very high resolution worldview 2 imagery," *Int. J. Appl. Earth Obs. Geoinf.,* vol. 26, pp. 298–311, 2014.

[47] H. Han *et al.*, "Detection of convective initiation using meteorological imager onboard communication, ocean, and meteorological satellite based on machine learning approaches," *Remote Sens,* vol. 7, no. 7, pp. 9184–9204, 2015.

[48] M. Jia *et al.*, "Tracking long-term floodplain wetland changes: A case study in the China side of the Amur river basin," *Int. J. Appl. Earth Obs. Geoinf.,* vol. 92, 2020, Art. no. 102185.

[49] T. Wang, H. Zhang, H. Lin, and C. Fang, "Textural–spectral feature-based species classification of mangroves in Mai Po nature reserve from worldview-3 imagery," *Remote Sens.,* vol. 8, no. 1, 2016, Art. no. 24.

[50] S. Morell-Monzó, J. Estornell, and M. Sebastiá-Frasquet, "Comparison of Sentinel-2 and high-resolution imagery for mapping land abandonment in fragmented areas," *Remote Sens.,* vol. 12, no. 12, 2020, Art. no. 2062.

[51] R. M. Haralick, K. Shanmugam, and I. Dinstein, "Textural features for image classification," *IEEE Trans. Power Syst.,* vol. SMC-3 no. 6, pp. 610–621, Nov. 1973.

[52] M. Clark, "Comparison of multi-seasonal Landsat 8, Sentinel-2 and hyperspectral images for mapping forest alliances in northern california," *ISPRS-J. Photogramm. Remote Sens.,* vol. 159, pp. 26–40, 2020.

[53] D. Wang *et al.*, "Evaluating the performance of Sentinel-2, Landsat 8 and Pléiades-1 in mapping mangrove extent and species," *Remote Sens.*, vol. 10, no. 9, 2018, Art. no. 1468.

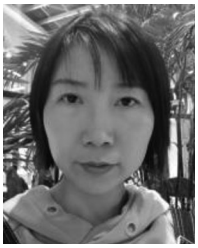

Rong Zhang received the M.S. degree in geomatics science and technology from Liaoning Technical University, Fuxin, China in 2019. She is currently working toward the Ph.D. degree in cartography and geography information system with the Northeast Institute of Geography and Agroecology, Chinese Academy of Sciences, Changchun, China.

Her current research interests include MFs remote sensing, multisource remote sensing, and coastal environmental studies, concentrating on mangrove species classification, machine learning and estimation of biophysical parameters of MFs using multispectral remote sensing images.

Mingming Jia received the Ph.D. degree in cartography and geographic information system from the University of Chinese Academy of Sciences, Beijing, China, in 2014.

She is a Research Assistant with the Key Laboratory of Wetland Ecology and Environment, Northeast Institute of Geography and Agroecology, Chinese Academy of Sciences. Her research interests include understanding the structure and function of mangrove species succession, exploring MFs changes under the influence of human and natural factors, such as reclamation, sea level rise, extreme weather events, and biological invasion, and evaluating carbon cycling and storage in MF.

Zongming Wang received the Ph.D. degree in environmental sciences from the Graduate University of Chinese Academy of Sciences, Beijing, China, in 2005.

He is a Professor with the Key Laboratory of Wetland Ecology and Environment, Northeast Institute of Geography and Agroecology, Chinese Academy of Sciences. He is the coauthor of more than 100 journal papers. His research interests include remote sensing of wetlands and regional environmental changes.

Yaming Zhou received the M.S. degree in cartography and geography information system from Xi'an University of Science And Technology, Xi'an, China in 2015.

She is currently an intermediate Engineer with the Ministry of Ecology and Environment Center for Satellite Application on Ecology and Environment, Beijing, China. She is mainly engaged in services for water environment remote sensing applications.

Xin Wen received the B.S. degree in land resource management from Jilin University, Changchun, China in 2018. She is currently working toward the M.S. degree in land resource management with Jilin University, Changchun, China.

Her current research interests include MFs remote sensing and coastal environmental studies, concentrating on mangrove species classification, machine learning and estimation of biophysical parameters of MFs using multispectral remote sensing images.

Yue Tan received the B.S. degree in geomatics engineering from Jilin Jianzhu University, Changchun, China, in 2019. She is currently working toward the M.S. degree in architectural and civil engineering with Jilin Jianzhu University, Changchun, China.

Her current research interests include MFs remote sensing and hydrophytic vegetation remote sensing, concentrating on mangrove species classification, machine learning.

Lina Cheng received the B.S. degree in geomatics engineering from Jilin Jianzhu University, Changchun, China in 2019. She is currently working toward the M.S. degree in land resource management with Jilin University, Changchun, China.

Her current research interests include MFs remote sensing and coastal environmental studies, concentrating on mud flats classification, and machine learning.